S14

Supporting Information for "Ganymede MHD Model: Magnetospheric Context for Juno's PJ34 Flyby"

Stefan Duling[1], Joachim Saur[1], George Clark[2], Frederic Allegrini[3], Thomas Greathouse[3], Randy Gladstone[3,4], William Kurth[5], John E. P. Connerney[6,7], Fran Bagenal[8], Ali H. Sulaiman[9]

[1]Institute of Geophysics and Meteorology, University of Cologne, Cologne, Germany
[2]The Johns Hopkins University Applied Physics Laboratory, Laurel, Maryland, USA
[3]Southwest Research Institute, San Antonio, Texas, USA
[4]University of Texas at San Antonio, San Antonio, Texas, USA
[5]Department of Physics and Astronomy, University of Iowa, Iowa City, Iowa, USA
[6]NASA Goddard Space Flight Center, Greenbelt, Maryland, USA
[7]Space Research Corporation, Annapolis, Maryland, USA
[8]Laboratory for Atmospheric and Space Physics, University of Colorado, Boulder, Colorado, USA
[9]School of Physics and Astronomy, Minnesota Institute for Astrophysics, University of Minnesota, Minneapolis, Minnesota, USA

Contents of this file

1. Text S1 to S4
2. Caption for Movie S5

Additional Supporting Information (Files uploaded separately)

1. Movie S5

Introduction

In S1 we provide a detailed description of the magnetohydrodynamic (MHD) model that was used to obtain the results presented in the article. In S2 we discuss the upstream conditions and other model parameters and their uncertainties. In S3 we describe details of the simulation code PLUTO and the numerical setup used in this analysis. In S4 we shortly compare the results from our independent simulation codes PLUTO and ZEUS-MP, solving the identical physical problem and discuss the impact of the spatial resolution. S5 is a movie that visualizes the modeled three-dimensional context of Juno's trajectory during its PJ34 flyby.

S1. Model Description

Ganymede's magnetosphere has been modeled with different physical approaches and numerical solvers. While multi-fluid (e.g. Paty, 2004; Wang et al., 2018), particle-in-cell (Tóth et al., 2016) and hybrid models (Fatemi et al., 2016; Romanelli et al., 2022) are primarily excellent for analyzing individual magnetospheric aspects or particle related physics, single fluid magnetohydrodynamic (MHD) (e.g. Jia et al., 2008; Duling et al., 2014) and Hall-MHD (e.g. Dorelli et al., 2015) models generally allow a higher spatial resolution for numerical reasons and therefore are well suited to model the global interaction topology.

We describe Ganymede's space environment by adopting a MHD model. Since the upstream conditions in Jupiter's magnetosphere can be assumed constant during the time scales of the local interaction at Ganymede the model approaches a steady-state solution. In our single-fluid approach the plasma interaction is described by the plasma mass density ρ, plasma bulk velocity $\mathbf{v}$, total thermal pressure p and the magnetic field $\mathbf{B}$. For these variables the MHD equations read in their conservational form, complemented by source terms on their right-hand sides:

$$\frac{\partial \rho}{\partial t} + \nabla \cdot \Big[\rho \mathbf{v}\Big] = P m_n - L m_L, \tag{1}$$

$$\frac{\partial \rho \mathbf{v}}{\partial t} + \nabla \cdot \Big[\rho \mathbf{v}\mathbf{v} - \frac{1}{\mu_0}\mathbf{B}\mathbf{B} + \mathbf{I}(p + \frac{1}{2}\frac{B^2}{\mu_0})\Big] = -(L m_L + \nu_n \rho)\mathbf{v}, \tag{2}$$

$$\frac{\partial E_t}{\partial t} + \nabla \cdot \Big[(E_t + p + \frac{1}{2}\frac{B^2}{\mu_0})\mathbf{v} - \frac{1}{\mu_0}\mathbf{B}(\mathbf{v}\cdot\mathbf{B})\Big] = -\frac{1}{2}(L m_L + \nu_n \rho)v^2 - \frac{3}{2}(L m_L + \nu_n \rho)\frac{p}{\rho} + \frac{3}{2}(P m_n + \nu_n \rho)\frac{k_B T_n}{m_n}, \tag{3}$$

$$\frac{\partial \mathbf{B}}{\partial t} - \nabla \times \Big[\mathbf{v} \times \mathbf{B}\Big] = 0. \tag{4}$$

The total energy $E_t = \frac{1}{2}\rho v^2 + \frac{3}{2}p + \frac{1}{2}\frac{B^2}{\mu_0}$ is composed of the kinetic, thermal and magnetic energy. The model features approximations of physical processes that build on the model of Duling et al. (2014). Momentum loss due to particle collisions with neutral O_2 molecules is characterized by a collision frequency ν_n as a function of a radially symmetric atmospheric particle density n_n. For expected plasma velocities $v_0 = 140$ km s^{-1} we adopt a constant cross section $\sigma_n = 2.2 \times 10^{-19}$ m^2:

$$\nu_n(r) = \sigma_n v_0 n_n(r). \tag{5}$$

The atmosphere is approximated with a hydrostatic model using a surface density of $n_{n,0} = 8.0 \times 10^{12}$ m^{-3}, a constant scale height of $H = 250$ km and Ganymede's radius $R_G = 2631$ km:

$$n_n(r) = n_{n,0} \exp\left(\frac{R_G - r}{H}\right). \tag{6}$$

Photo-ionization of the atmospheric particles as well as recombination in areas of high density are characterized by the production rate P and loss rate L respectively. We characterize the photo-ionization by an ionization rate $\nu_{ion} = 2.2 \times 10^{-8}$ s^{-1}:

$$P(r) = \nu_{ion} n_n(r). \tag{7}$$

The dissociative recombination is parameterized by a recombination rate coefficient $\alpha = 7.8 \times 10^{-14}$ m^3 s^{-1} and only active in regions with higher plasma density than the upstream value ρ_0:

$$L = \begin{cases} \alpha \rho (\rho - \rho_0) m_L^{-2} & \text{for } \rho > \rho_0 \\ 0 & \text{else} \end{cases} \tag{8}$$

These parameterizations are explained in detail in Duling et al. (2014). For all chemical processes we assume the mass of O_2 molecules $m_n = m_L = 32$ amu, neglecting the recently detected H_2O component on the sub-solar side (Roth et al., 2021). The last term in the energy equation (3) considers the transfer of thermal energy from the neutral atmosphere to the plasma. Since the thermal energy of the atmosphere is low compared to the plasma, this term is expected to be negligible. We keep it for completeness and set the atmosphere's temperature to $T_n = 100$ K (Marconi, 2007) while k_B is the Boltzmann constant.

Ganymede's intrinsic magnetic field is described by dipole Gauss coefficients $g_1^0 = -716.8$ nT, $g_1^1 = 49.3$ nT, $h_1^1 = 22.2$ nT as derived by Kivelson, Khurana, and Volwerk (2002). Within their uncertainties, dipole coefficients updated from Juno data by Weber et al. (2022) have equal values. Quadrupole models either neglect an induction

response of an ocean (Saur et al., 2013) or do not significantly improve the fit to available data. In our model we include an induced dipole moment in the equatorial plane:

$$\begin{pmatrix} g^1_{1,\mathrm{ind}}(\lambda_{\mathrm{III}}) \\ h^1_{1,\mathrm{ind}}(\lambda_{\mathrm{III}}) \end{pmatrix} = 0.5A \begin{pmatrix} B_{0,y}(\lambda_{\mathrm{III}}+\Phi) \\ -B_{0,x}(\lambda_{\mathrm{III}}+\Phi) \end{pmatrix} \left(\frac{R_T}{R_G}\right)^3. \tag{9}$$

Depending on the ocean model the induction response is characterized by the factor A and phase Φ (Duling et al., 2014), System-III longitude $\lambda_{\mathrm{III}} = 302°$, top radius of the ocean $R_T = 2481$ km and the inducing field

$$B_{0,x}(\lambda_{\mathrm{III}}) = -18\mathrm{nT}\sin(\lambda_{\mathrm{III}} - 200°), \tag{10}$$

$$B_{0,y}(\lambda_{\mathrm{III}}) = -86\mathrm{nT}\cos(\lambda_{\mathrm{III}} - 200°). \tag{11}$$

During Juno's visit Ganymede was near the center of the current sheet where the induction response is close to minimum. The corresponding factor $A = 0.95$ and phase $\Phi = -7°$ result in a maximum surface strength of the induced dipole of 15.6 nT.

The occurrence of magnetic reconnection has been confirmed at Ganymede (Ebert et al., 2022; Romanelli et al., 2022). To adequately model reconnection the consideration of finite plasma conductivity at the magnetopause is necessary. Theoretically, our model allows the addition of a physical resistivity term to the induction equation 4. In a simulation with lower grid resolution (50-250 km cell size inside the magnetosphere) we included anomalous and ionospheric resistivity similar to Duling et al. (2014) and Jia, Walker, Kivelson, Khurana, and Linker (2009) and have not found any significant impact on the magnetic topology at all. The strongest deviations from the same simulation without physical resistivity were <1 nT for the magnetic field on Juno's trajectory and <0.1° for the OCFB surface location. To reduce the computing time of simulations with high grid resolution (S3) and make extensive parameter studies possible we therefore deactivated the resistivity term for the presented study. The always present numerical resistivity, that results from the discretization of space and time and depends on the solver, reduces with higher grid resolution. However, by increasing the resolution we found that the solution globally converges to better fit the measurements, suggesting better results with reduced resistivity (Section S4). Therefore we still expect the impact of the physical resistivity on the high resolution simulations would be low and insignificant for the results of this study.

S2. Upstream Conditions and Model Parameters

Our model uses homogeneous and steady-state upstream conditions that are adjusted to the situation during Juno's flyby. Most of the values are not available yet from direct measurements. Therefore we use empirical or modeled predictions which have uncertainties of different order. To assess the model sensitivity on these parameter uncertainties (Section 4) we consider the minimum and maximum realistic values.

An appropriate value for Jupiter's magnetospheric field at the location of Ganymede can directly be obtained from measurements of the magnetometer on-board Juno. Therefore the undisturbed field measurements before ((-16,3,-70) nT) and after ((-14,43,-80) nT) the flyby (Weber et al., 2022) have to be interpolated to obtain a value suitable for the situation during CA ((-15,24,-75) nT). This value has some uncertainties because the temporal change is possibly non-linear and the convection time might play a role as well. The measurements before and after CA are nevertheless most likely upper and lower limits for the magnetic field.

Upstream plasma conditions are more difficult to determine. Juno's JADE and JEDI instruments provide particle distribution functions which in theory enable numerical moment calculations to achieve the plasma density, velocity and thermal pressure. However, at the moment numerical moments do not provide reliable values. Until refined analysis might help to determine those upstream conditions in the future, we access predictions. The plasma velocity relative to Ganymede depends on how strongly Jupiter's magnetosphere sub-corotated during the flyby. Voyager and Galileo data suggest a relative velocity of 140 km/s with a variability of 20 km/s (Kivelson et al., 2022). The density is expected to vary by a factor of 5 depending on Ganymede's position with respect to the current sheet (Jia et al., 2008), whereas literature values reveal larger uncertainties: 54 amu/cm^3 on average with a variability of 2-100 amu/cm^3 (Kivelson et al., 2004), 30 (13-46) amu/cm^3 with an uncertainty factor of 2 (Bagenal & Delamere, 2011), 160 amu/cm^3 inside the current sheet and 48 amu/cm^3 on higher magnetic latitudes (Kivelson et al., 2022). JADE measured 1 cm^{-3} protons and 8 cm^{-3} heavy ions before the flyby (Allegrini et al., 2022), consistent with electron densities of 5-12 cm^{-3} observed by the Waves instrument outside of the magnetosphere (Kurth et al., 2022). We assume 100 amu/cm^3 for our model and investigate the effects of extreme densities 10 and 160 amu/cm^3. The thermal pressure is dominated by energetic particles in the vicinity of Ganymede (Mauk, 2004). Therefore JEDI measurements provide a lower limit to the pressure during the flyby. Clark et al. (2022) calculated 1.5 nPa for the >50 keV protons. Sulfur and oxygen are expected to have a significant but unknown contribution. Former models assumed 3.8 nPa (Jia et al., 2008; Duling et al., 2014), here we use 2.8 nPa as also specified by Kivelson et al. (2022) and consider generous limits of 1.0 nPa and 5.0 nPa as uncertainties.

The best guess upstream conditions for our default model characterize the interaction to be sub-Alfvénic with an Alfvén Mach number of M_A =0.8, and a plasma beta of 1.1.

S3. Numerical Solution Process

We perform numerical simulations to obtain an approximate solution for equations (1-4). While we utilized the ZEUS-MP code (Hayes et al., 2006) for our former work, we now present results obtained with the PLUTO code (Mignone et al., 2007). This code is broadly used in the plasma science community and gives us the advantage to compare and validate our model results obtained by two different and independent numerical solvers. PLUTO is an open-source software designed to solve hyperbolic and parabolic systems of PDE's for astrophysical fluid dynamics. In contrast to ZEUS-MP's finite difference approach it uses the finite volume method. In our application we utilize a piece-wise linear, 2nd order reconstruction of the variables in the cells, the Harten, Lax, Van Leer solver for the Riemann problem to calculate the fluxes at the cell interfaces and a 2nd order Runge Kutta scheme for the integration forward in time. Unfeasible time steps and instabilities caused by possibly emerging vacuums are prevented by ensuring a minimal mass density and thermal pressure of 5% of the upstream value.

For the numerical solution we divide the space between Ganymede's surface and 70 Ganymede radii (R_G) into a grid with spherical geometry and a longitudinal resolution of 1.4°. To adequately resolve the strong magnetic tension in the equatorial region we use a latitudinal resolution of 0.74° between 26°N/S and 1.4° at the poles. Below 1.2 R_G the radial resolution equals 0.017 R_G and increases afterwards smoothly in the region below 12 R_G and steeply afterwards. Near the magnetopause at $\sim$ 2 R_G the radial cell distance is 0.025 R_G, at 12 R_G it is 0.12 R_G and at the outer boundary at 70 R_G it is 1.7 R_G. With a radial and latitudinal resolution of <65km inside the magnetosphere the grid is able to resolve the ion inertial length ($\sim$320km) (Dorelli et al., 2015). The cell number resolution is 308×208×256 (r, θ, ϕ) resulting in 16.4 million cells in total.

Representing Ganymede's surface, the inner boundary absorbs the incoming plasma. This is considered by applying open conditions for the plasma variables in addition to forcing the radial velocity component to be zero or negative. Ganymede's icy, electrically non-conducting crust cannot carry electric currents. This property directly affects the near surface magnetic field and is considered through isolating boundary conditions derived in Duling et al. (2014). At the outer boundary we use fixed boundary values equal to the upstream conditions on the upstream side and open conditions on the downstream side.

S4. Impact of Solver and Resolution on the Results

In addition to the PLUTO code (Mignone et al., 2007), applied in this work, we previously modeled Ganymede with the ZEUS-MP code (Hayes et al., 2006). This gives us the unique opportunity to compare the results of identical models setups numerically calculated with two independent solvers. However, using the high spatial resolution of this study with ZEUS-MP exceeds the technical resources we have available. Therefore we performed lower resolution simulations with both codes for the identical model described in Section S1 and our default parameter set. In this comparison we use 2.1 million cells in total, the minimal radial resolution is 0.02 R_G and the constant latitudinal and longitudinal resolutions are 2.8°.

Table S1. Results for the identical physical model obtained from independent simulation codes for different spatial resolutions. Columns 3-6 specify the averaged latitude of the northern and southern open closed field line boundary (OCFB) on Ganymede's surface on the upstream (-45° to -135°W) and downstream (45° to 135°W) side. Column 7 lists Juno's closest distance to closed field lines (CF) and columns 8-9 the UTC times of its inbound and outbound magnetopause crossings, respectively. Column 10 lists the RMS between measured and modeled magnetic field between 16:50 and 16:59.

Table S1.

		OCFB down		OCFB up		CF	magnetopause crossing		RMS
code	resolution	N [°]	S [°]	N [°]	S [°]	[R_G]	inbound	outbound	[nT]
PLUTO[a]	high	21.2	-24.4	51.5	-47.4	0.26	16:48:16	17:00:16	9.3
PLUTO	low	27.6	-30.8	54.3	-50.3	0.13	16:49:25	17:00:26	23.5
ZEUS-MP	low	28.1	-31.2	56.4	-51.8	0.02	16:48:50	17:00:00	26.9

[a]: default model of the main study

In Figures S1 and S2, similar to Figures 3 and 4 of the main study, we present the results of PLUTO (green) and ZEUS-MP (orange) together with the PLUTO results with the higher resolution of the main study (dashed green). Table S1 lists selected quantitative results. First, we shortly analyze the effect of a reduced spatial resolution by considering only the results from PLUTO. In general the modeled magnetic field fits the observations worse than with the high resolution, especially the B_z component (Figure S1c) at the inbound field rotation (16:45) and near the closed field line region around CA. Additionally the OCFB on Ganymede's surface is shifted polewards (Figure S2) for all longitudes, indicating a larger closed field line region. As consequence the closest distance to closed field lines (Figure S1e) is reduced, but Juno is still not entering the closed field line region. An effect of

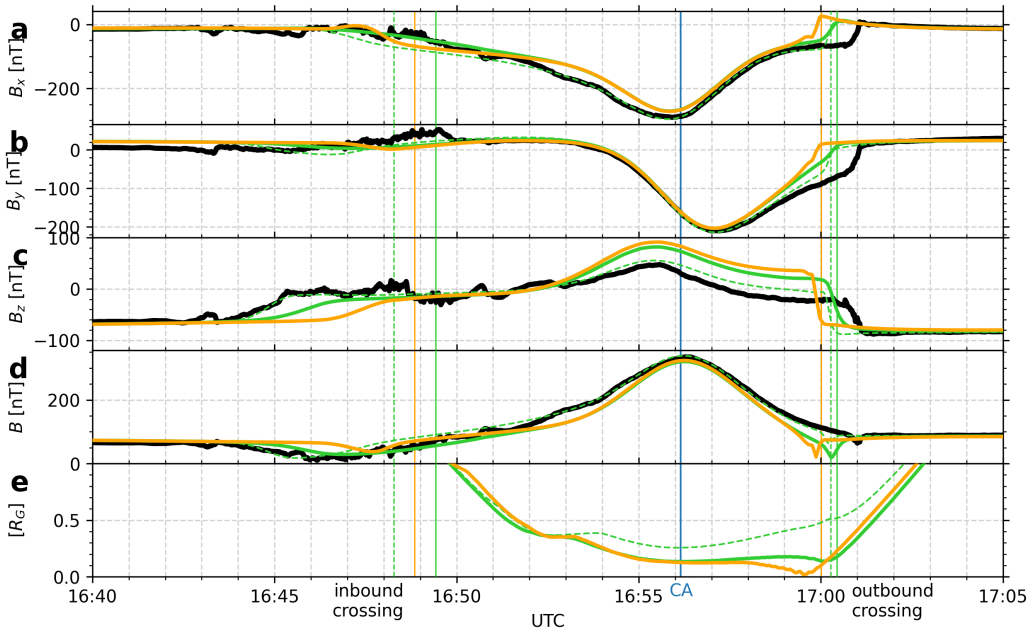

Figure S1. Modeled magnetic field along Juno's trajectory from PLUTO (green) and ZEUS-MP (orange) for the identical physical model and reduced spatial resolution. The magnetic field from the default model with higher resolution of the main study is shown as dashed green lines, Juno's measurements in black. Panels a-c show GPhiO components, panel d the magnitude. Panel e shows Juno's distance from the OCFB in R_G. The vertical lines represent the modeled inbound and outbound magnetopause crossings.

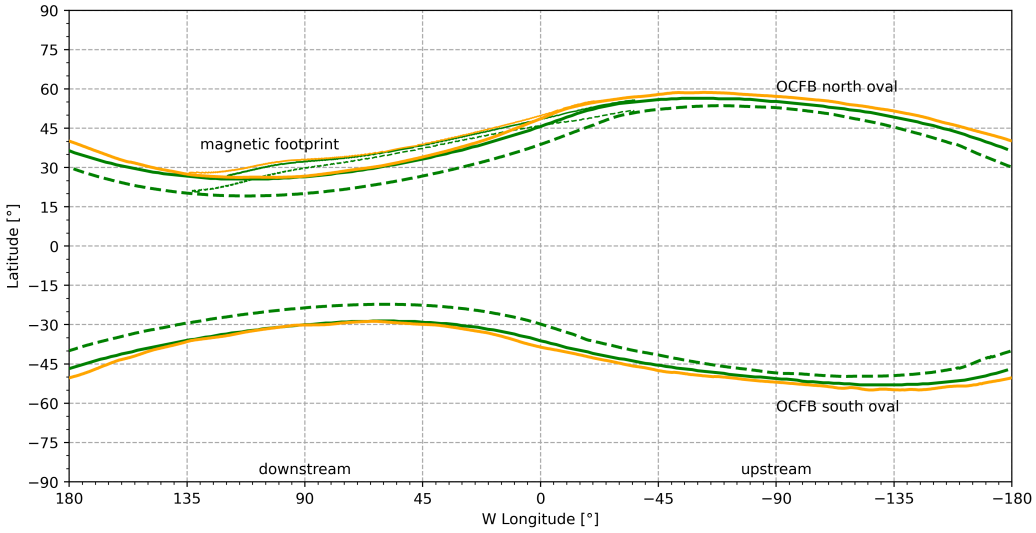

Figure S2. Surface map of Ganymede with 0° western longitude pointing towards Jupiter (+y axis GPhiO). The OCFB (thick) and Juno's magnetic footprint (thin) from PLUTO (green) and ZEUS-MP (orange) but the identical physical model are shown for a reduced spatial resolution. The results from the default model of the main study are shown as dashed green lines.

a reduced spatial resolution is the increase of the numerical resistivity. The code becomes more diffusive and as consequence boundary layers become less sharp pronounced, magnetic tension is less preserved and the closed field line region expands. Since the high resolution results fit the observations very well we expect a weaker resistivity to improve the fit and the high resolution to be sufficient to model the Juno flyby. However, the location of the outbound magnetopause crossing (Figure S1, ∼17:00:26) is better modeled with the lower resolution, even though the shape of the magnetic field rotation is worse. As discussed in the main study the outbound magnetopause crossing remains an open question.

Comparing the results from PLUTO and ZEUS-MP for the low resolution we find similar results. The OCFB on Ganymede's surface (S2) has differences between 5° at the anti-Jovian side and <1° at the downstream side where Juno mainly observed the aurora. The OCFB from ZEUS-MP is located polewards of the OCFB from PLUTO which is also reflected in Juno's slightly lower distance to closed field lines in the case of ZEUS-MP (Figure S1e). The modeled magnetic field from ZEUS-MP (Figure S1c) also has a slightly worse fit to the field rotation in the wake region (around 16:45) and the outbound magnetopause crossing. All these discrepancies suggest that ZEUS-MP might be slightly more resistive than PLUTO. For the major parts of Juno's trajectory, however, both independent codes produce very similar results, suggesting additional reliability of our numerical implementations. The primary purpose of this comparison is that the remaining differences give an impression of the numerical error that can be expected while modeling Ganymede's magnetosphere.

S5. Movie

The movie illustrates the three-dimensional geometry of Ganymede's magnetosphere in reference to Juno's trajectory (red line) for the time around closest approach. The green surface represents the extent of the closed field line region. The blue surfaces represent the regions with open field lines that connect Ganymede's polar regions with Jupiter and correspond to the Alfvén wings. The white tubes show selected closed and open field lines and the orange tubes show field lines that are seeded on Juno's trajectory. Outside of the magnetosphere these field lines are unconnected and inside the magnetosphere they end at Ganymede's surface, representing Juno's magnetic footprint. Auroral oxygen emissions are displayed on Ganymede's surface as observed by Juno's UVS instrument (Greathouse et al., 2022).

References

Allegrini, F., Bagenal, F., Ebert, R., Louarn, P., McComas, D. J., Szalay, J., ... Waite, J. H. (2022). Plasma observations during the june 7, 2021 ganymede flyby from the jovianauroral distributions experiment (jade) on juno. *Geophysical Research Letters*, *this issue*.

Bagenal, F., & Delamere, P. A. (2011, may). Flow of mass and energy in the magnetospheres of jupiter and saturn. *Journal of Geophysical Research: Space Physics*, *116*(A5). doi: 10.1029/2010ja016294

Clark, G., Mauk, B. H., Paranicas, C., Kollmann, P., Haggerty, D., Rymer, A., ... Turner, D. L. (2022). Energetic charged particle observations during juno's close flyby of ganymede. *Geophysical Research Letters*, *this issue*.

Dorelli, J. C., Glocer, A., Collinson, G., & Tóth, G. (2015, jul). The role of the hall effect in the global structure and dynamics of planetary magnetospheres: Ganymede as a case study. *Journal of Geophysical Research: Space Physics*, *120*(7), 5377–5392. doi: 10.1002/2014ja020951

Duling, S., Saur, J., & Wicht, J. (2014, jun). Consistent boundary conditions at nonconducting surfaces of planetary bodies: Applications in a new ganymede MHD model. *Journal of Geophysical Research: Space Physics*, *119*(6), 4412–4440. doi: 10.1002/2013ja019554

Ebert, R. W., Fuselier, S., Allegrini, F., Angold, N., Bagenal, F., Bolton, S. J., ... Wilson, R. J. (2022). Evidence for magnetic reconnection at ganymede's upstream magnetopause during the pj34 juno flyby. *Geophysical Research Letters*, *this issue*.

Fatemi, S., Poppe, A. R., Khurana, K. K., Holmström, M., & Delory, G. T. (2016, may). On the formation of ganymede's surface brightness asymmetries: Kinetic simulations of ganymede's magnetosphere. *Geophysical Research Letters*, *43*(10), 4745–4754. doi: 10.1002/2016gl068363

Greathouse, T. K., Gladstone, R., Molyneux, P. M., Versteeg, M. H., Hue, V., Kammer, J., ... Duling, S. (2022). Uvs observations of ganymede's aurora during juno orbits 34 and 35. *Geophysical Research Letters*, *this issue*.

Hayes, J. C., Norman, M. L., Fiedler, R. A., Bordner, J. O., Li, P. S., Clark, S. E., ... Low, M.-M. M. (2006, jul). Simulating radiating and magnetized flows in multiple dimensions with ZEUS-MP. *The Astrophysical Journal Supplement Series*, *165*(1), 188–228. doi: 10.1086/504594

Jia, X., Walker, R. J., Kivelson, M. G., Khurana, K. K., & Linker, J. A. (2008, jun). Three-dimensional MHD simulations of ganymede's magnetosphere. *Journal of Geophysical Research: Space Physics*, *113*(A6), n/a–

n/a. doi: 10.1029/2007ja012748
Jia, X., Walker, R. J., Kivelson, M. G., Khurana, K. K., & Linker, J. A. (2009, sep). Properties of ganymede's magnetosphere inferred from improved three-dimensional MHD simulations. *Journal of Geophysical Research: Space Physics*, *114*(A9), n/a–n/a. doi: 10.1029/2009ja014375
Kivelson, M. G., Bagenal, F., Jia, X., Khurana, K., Volwerk, M., & Zarka, P. (2022). Ganymede's magnetosphere and its interaction with the jovian magnetosphere. In M. Volwerk & M. McGrath (Eds.), *Ganymede.* Cambridge, UK: Cambridge University Press.
Kivelson, M. G., Bagenal, F., Kurth, W. S., Neubauer, F. M., Paranicas, C., & Saur, J. (2004). Magnetispheric interaction with satellites. In *Jupiter - the planet, satellites and magnetosphere* (p. 513-536). Cambridge Univ. Press, New York.
Kivelson, M. G., Khurana, K., & Volwerk, M. (2002, jun). The permanent and inductive magnetic moments of ganymede. *Icarus*, *157*(2), 507–522. doi: 10.1006/icar.2002.6834
Kurth, W., Sulaiman, A., Hospodarsky, G. B., Menietti, J., Mauk, B. H., Clark, G., ... Louis, C. (2022). Juno plasma wave observations at ganymede. *Geophysical Research Letters*, *this issue*.
Marconi, M. (2007, sep). A kinetic model of ganymede's atmosphere. *Icarus*, *190*(1), 155–174. doi: 10.1016/j.icarus.2007.02.016
Mauk, B. H. (2004). Energetic ion characteristics and neutral gas interactions in jupiter's magnetosphere. *Journal of Geophysical Research*, *109*(A9). doi: 10.1029/2003ja010270
Mignone, A., Bodo, G., Massaglia, S., Matsakos, T., Tesileanu, O., Zanni, C., & Ferrari, A. (2007, may). PLUTO: A numerical code for computational astrophysics. *The Astrophysical Journal Supplement Series*, *170*(1), 228–242. doi: 10.1086/513316
Paty, C. (2004). Multi-fluid simulations of ganymede's magnetosphere. *Geophysical Research Letters*, *31*(24). doi: 10.1029/2004gl021220
Romanelli, N., DiBraccio, G. A., Modolo, R., Connerney, J. E. P., W.Ebert, R., Martos, Y. M., ... Bolton, S. J. (2022). Analysis of juno magnetometer observations:comparisons with a global hybrid simulation andindications of ganymede's magnetopause reconnection. *Geophysical Research Letters*, *this issue*.
Roth, L., Ivchenko, N., Gladstone, G. R., Saur, J., Grodent, D., Bonfond, B., ... Retherford, K. D. (2021, jul). A sublimated water atmosphere on ganymede detected from hubble space telescope observations. *Nature Astronomy*, *5*(10), 1043–1051. doi: 10.1038/s41550-021-01426-9
Saur, J., Grambusch, T., Duling, S., Neubauer, F. M., & Simon, S. (2013, apr). Magnetic energy fluxes in sub-alfvénic planet star and moon planet interactions. *Astronomy & Astrophysics*, *552*, A119. doi: 10.1051/0004-6361/201118179
Tóth, G., Jia, X., Markidis, S., Peng, I. B., Chen, Y., Daldorff, L. K. S., ... Dorelli, J. C. (2016, feb). Extended magnetohydrodynamics with embedded particle-in-cell simulation of ganymede's magnetosphere. *Journal of Geophysical Research: Space Physics*, *121*(2), 1273–1293. doi: 10.1002/2015ja021997
Wang, L., Germaschewski, K., Hakim, A., Dong, C., Raeder, J., & Bhattacharjee, A. (2018, apr). Electron physics in 3-d two-fluid 10-moment modeling of ganymede's magnetosphere. *Journal of Geophysical Research: Space Physics*, *123*(4), 2815–2830. doi: 10.1002/2017ja024761
Weber, T., Moore, K., Connerney, J., Espley, J., DiBraccio, G., & Romanelli, N. (2022). Updated spherical harmonic moments of ganymedefrom the juno flyby. *Geophysical Research Letters*, *this issue*.